American Mineralogist, Volume 77, pages 758–764, 1992

Cylindrite: The relation between its cylindrical shape and modulated structure

Su Wang, Peter R. Buseck
Departments of Geology and Chemistry, Arizona State University, Tempe, Arizona 85287, U.S.A.

Abstract

Cylindrite, a lead, tin, antimony, iron sulfosalt having a distinctive cylindrical morphology and a composite structure, is characterized by incommensurate structural modulations. It contains two types of sheets, and these have pseudohexagonal (H) and pseudotetragonal (T) structures with distinct lattice dimensions. The structure changes systematically from core to periphery of the crystals. The **b** and **c** axes of the H and T sheets are almost parallel to each other near the crystal cores. Further from the cores the angular divergence between the axes of the two types of sheets increases (i.e., the sheets are increasingly rotated relative to one another), and the wavelength of the structural modulation decreases. The crystal accommodates the dimensional misfit between the H and T sheets by a combination of this divergence, the variation of the structural modulation, and the curving of the layers.

Introduction

Crystals of almost all minerals form with flat faces, and these faces characteristically grow at sharp angles to one another. Cylindrite belongs to a select group of minerals that typically displays an anomalous morphology; as implied by its name, it forms in crystals shaped like cylinders. Although highly unusual, tubular forms are also adopted by a few other minerals, such as chrysotile (Yada, 1967, 1971; Veblen and Buseck, 1979), hollandite (Belkin and Libelo, 1987), and tochilinite (Tomeoka and Buseck, 1983; Zolensky and Mackinnon, 1986). However, individual crystals of these minerals are generally microscopic in dimensions. Because of their small sizes, it is difficult to obtain good diffraction patterns and images from different parts and orientations of the crystals to determine the relation between their morphologies and crystal structures. Cylindrite, in striking contrast, forms in crystals several millimeters in diameter, and these provide a good opportunity for understanding the structure of crystals with cylindrical morphology.

Makovicky (1971, 1974) examined cylindrite using scanning electron microscopy (SEM) and X-ray diffraction and showed that it forms in concentric, curved layers. The regular cylindrical structure is distorted within the cylinder cores so that it assumes horseshoelike forms (Fig. 1, arrow) or other irregular shapes. Makovicky (1974) proposed that the mineral consists of two types of structural sheets that alternate regularly, and he called them pseudotetragonal (T) and pseudohexagonal (H), reflecting their respective symmetries. The H sheet, with composition MS_2, essentially represents an octahedral $(Sn^{4+},Fe)S_2$ sheet with the berndtite (brucite-like) structure; the T sheet, with composition $(Pb,Sb,Sn^{2+})S$, represents two PbS layers with the galena structure. The lattice parameters of the two sheets, both of which are A centered, are given in Table 1; in spite of being intergrown, their axes are not exactly parallel to one another. The two types of sheets are unusual in that they have different structures and symmetries as well as incommensurate dimensions parallel to the layering. They stack along the **a*** direction in the sequence HTHT.

Crystallographic complications arise where crystals consist of two or more units having different structures (e.g., Evans and Allmann, 1968; Buseck and Veblen, 1988; Coppens et al., 1990; Petricek et al., 1991), and modulations commonly result (Cowley, 1979; Buseck and Cowley, 1983). The structural complexity increases in proportion to the degree of dimensional mismatch among the structural units. For comparison, in the serpentine minerals there is a relatively small mismatch (Table 2). The two types of sheets in serpentine are accommodated in any of three ways: (1) a curled structure is adopted, as in chrysotile; (2) a wave structure occurs, as in antigorite; (3) large cations are replaced by small cations, as in lizardite. In cylindrite, there is a larger structural mismatch (Table 2), and so serpentine-type mechanisms occur in combination. In the **b** direction, the layers curl into cylinders as in chrysotile, but no fixed dimensional relationship was observed between the two sheets. In the **c** direction, approximately parallel to the axis of the cylinders, high-resolution transmission electron microscopy (HRTEM) images show that the dimensions of the two sheets are in the approximate proportion $13c_t/12c_h$ (b_t, c_t and b_h, c_h represent the unit lengths of the **b** and **c** axes of the T and H sheets, respectively); they produce a match by forming modulated intergrowths, as in antigorite (Wang and Kuo, 1991; Wang, 1988; Williams and Hyde, 1988).

The cylindrite modulations give rise to satellite reflections in selected-area electron diffraction (SAED) patterns, and the vector **q**, which describes the modulation, is oriented parallel to these reflections in reciprocal space. If a diffraction vector, **H**, is described in terms of either

0003–004X/92/0708–0758$02.00

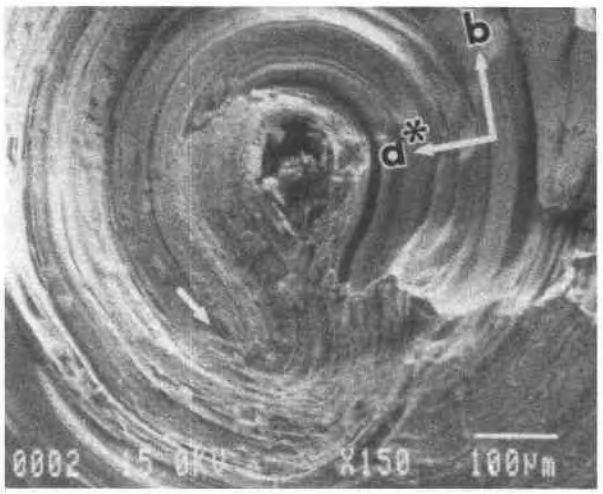

Fig. 1. SEM image of cylindrite showing the structure in the core of a cylindrical crystal.

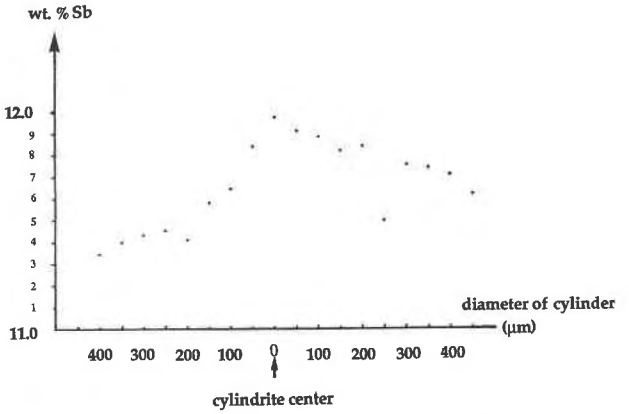

Fig. 2. The distribution of Sb across a cylindrite cylinder.

the H or T lattice parameters, then $\mathbf{H} = h\mathbf{a}^* + k\mathbf{b}^* + l\mathbf{c}^* + m\mathbf{q}$ (h, k, l, m are integers), where $\mathbf{q} = q_a\mathbf{a}^* + q_b\mathbf{b}^* + q_c\mathbf{c}^*$ (q_a, q_b, and q_c are coefficients; de Wolff et al., 1981). In cylindrite, q_a, q_b, and q_c do not have fixed rational values. Transmission electron microscope (TEM) observations showed that the orientational relations between the axes of the H and T sheets and between these sheets and the vector **q** are variable (Wang and Kuo, 1991), although the details of the variations were unclear.

The dimensional mismatch in the **b** direction, which is parallel to the tangent of the cylinders, is larger than that in the **c** direction. However, no structural modulations have been observed in the **b** direction. Specific questions examined in this paper are whether there are structural differences between cylindrite fragments having large vs. small radii of curvature, and how and why the relation between these sheets and the modulation vector **q** varies.

Specimens and experimental details

A cylindrical crystal with a 6-mm diameter, from Poopo, Bolivia, was used for TEM study. In order to contrast the structural differences between sheets that are close to the core of the crystal and those far from the center, fragments from the innermost, medial, and outermost parts of the cylinder were used for TEM observation. Electron-transparent foils oriented parallel to (100) were prepared for study by repeated cleaving (Hirsch et al., 1977). For observation of cylinder cross sections, slabs having about a 1-mm thickness were glued between two Si wafers with epoxy resin to make a sandwich. These sandwiches were then ground and polished perpendicular to the cylinder axis, thereby obtaining specimens 30 μm thick with orientation normal to the {100} cleavage planes. They were ion thinned using a Gatan 600 ion mill. A cooling stage was used to minimize damage during ion milling.

Secondary electron images and quantitative analyses were obtained with a JEOL JXA-8600 electron microprobe using a 10-nA beam current. Standard calibration procedures were employed using galena for Pb and S and the metals for Sn, Sb, and Fe, respectively. The electron-transparent foils were examined in an Akashi EM-002B TEM operated at 200 kV with a LaB_6 filament and equipped with a ±10° double-tilt, side-entry high-resolution goniometer stage. The spherical aberration coefficient, C_s, of the objective lens is 0.4 mm. Heating experiments were performed using a Philips EM 400T TEM at an accelerating potential of 120 kV.

Observations

Microprobe analyses were performed across the width of a 2-mm cylinder in order to determine whether compositional variations coincide with distance from the core.

Table 1. Lattice parameters of the sheets in the cylindrite structure

	H sheet	T sheet
a	1.173 nm	1.176 nm
b	0.367	0.579
c	0.632	0.581
α	91°	91°
β	91°	92°
γ	91°	95°

Note: *a*, *b*, *c* are from Makovicky (1974) and α, β, γ are from Wang and Kuo (1991).

Table 2. Comparison between the dimensions of the two types of sheets in the serpentine and cylindrite structures

Serpentine minerals	*a*	*b*
Si-O sheet	0.53 nm	0.92 nm
Brucite sheet	0.54	0.94 (3 × 0.313)
Difference	0.01	0.02
Cylindrite*	***b***	***c***
T sheet	0.579 nm	0.581 nm
H sheet	0.367	0.632
Difference	0.212	0.051

* Values for *b* and *c* are from Makovicky (1974).

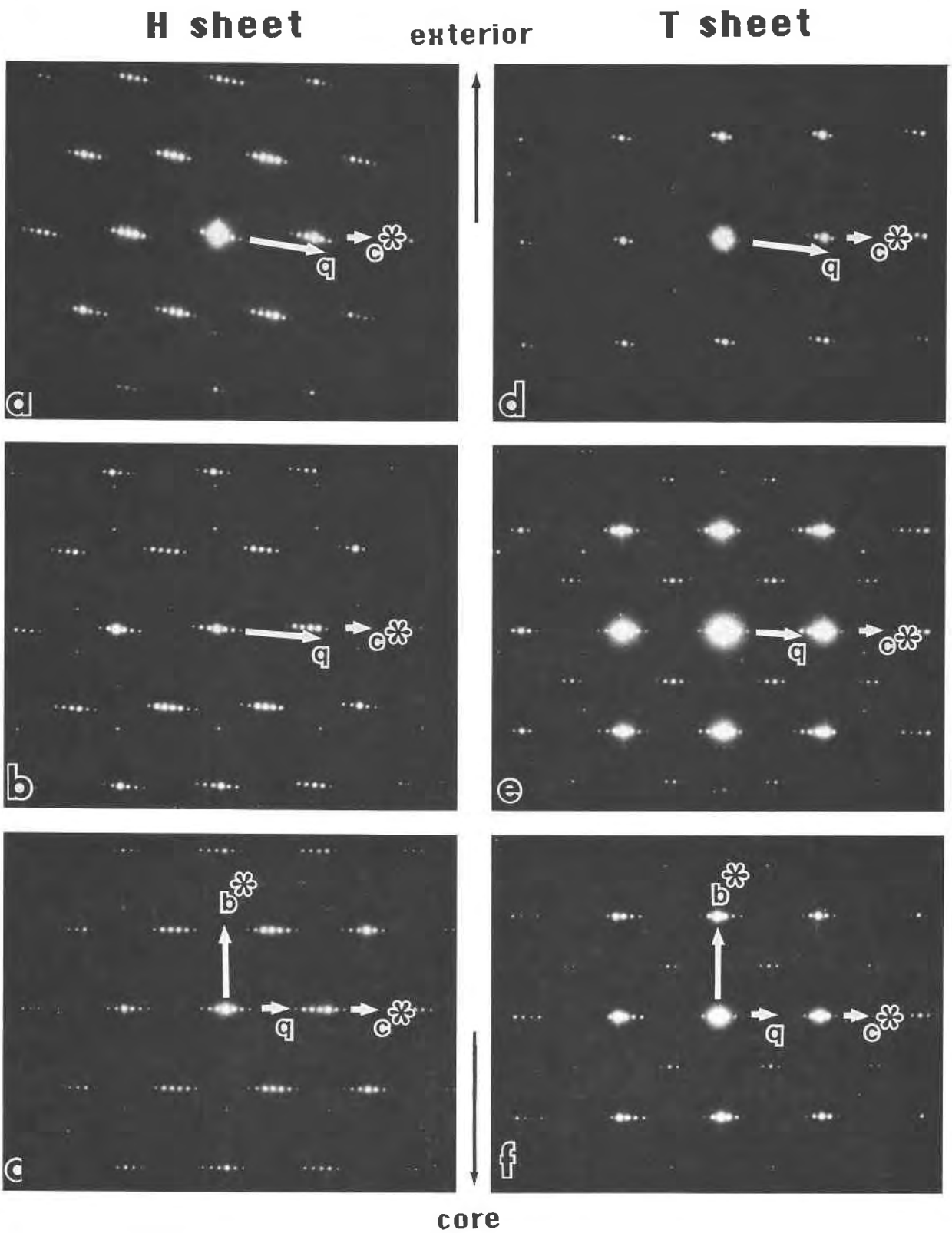

Fig. 3. Some [100] SAED patterns of cylindrite. (**a**), (**b**), (**c**) Patterns of the H sheets; (**d**), (**e**), (**f**) patterns of the T sheets. (**a**), (**d**) The outside edge of a cylinder; (**b**), (**e**) the middle of a cylinder; (**c**), (**f**) close to the cylinder core. The modulation vector is denoted by **q**.

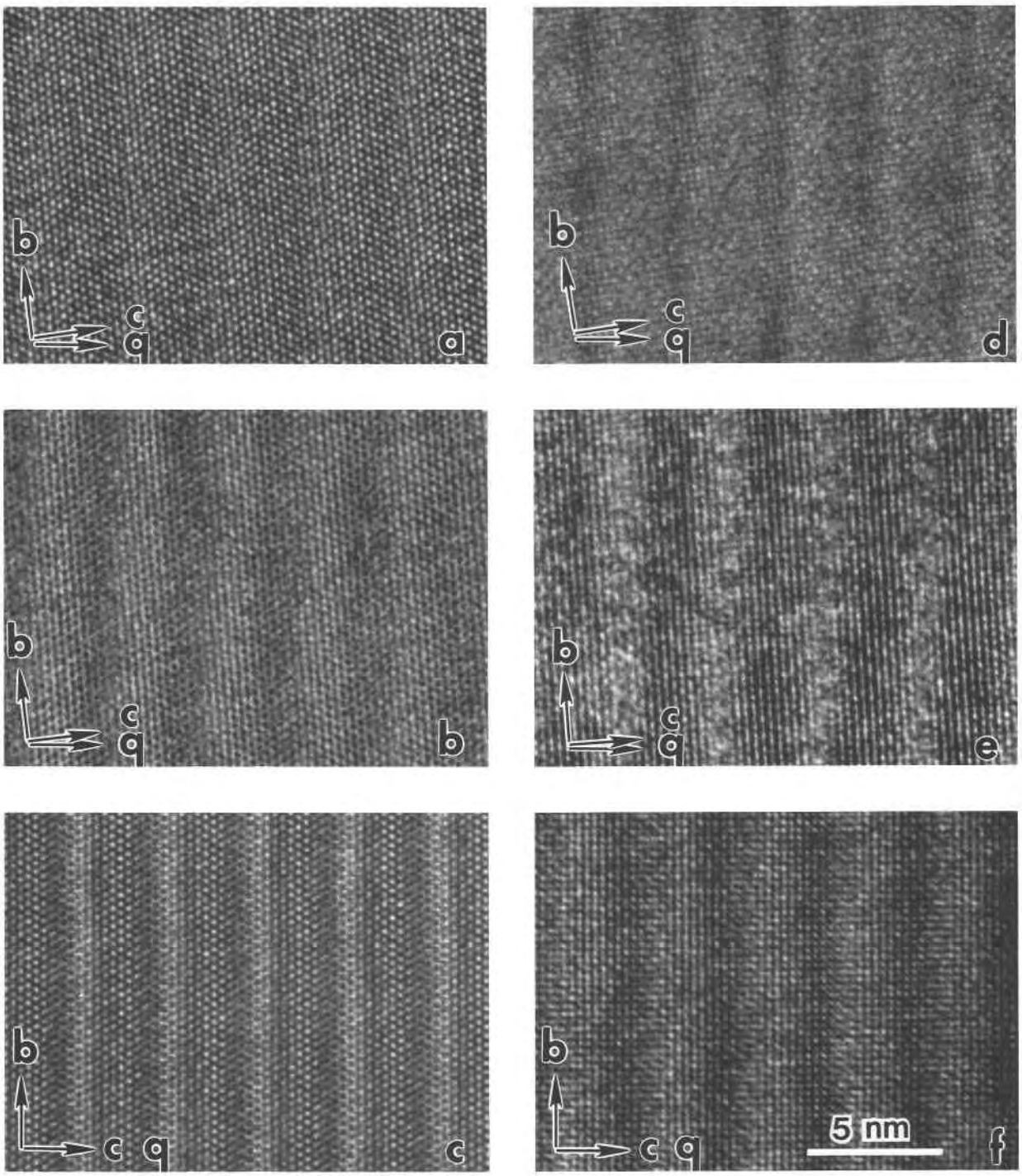

Fig. 4. Some [100] HRTEM images of cylindrite. The images correspond to the respective SAED patterns of Figure 3.

Concentrations of Fe, Sn, Sb, Pb, and S were measured with wavelength-dispersive spectrometers at 18 evenly spaced points at 50-μm intervals. The averages of these microprobe analyses, corresponding to the points in Figure 2, show the following weight percent values: S = 24.68, Fe = 2.70, Sn = 27.37, Sb = 11.68, and Pb = 33.72, giving a total of 100.15. Sb ranges from 12.03 wt% at the cylinder center to 11.39 at the periphery. Because the range is small and because we did not observe complementary, systematic variations in the other elements, the indicated zoning should be considered tentative.

There is a small angle between the **a** axes of the H and

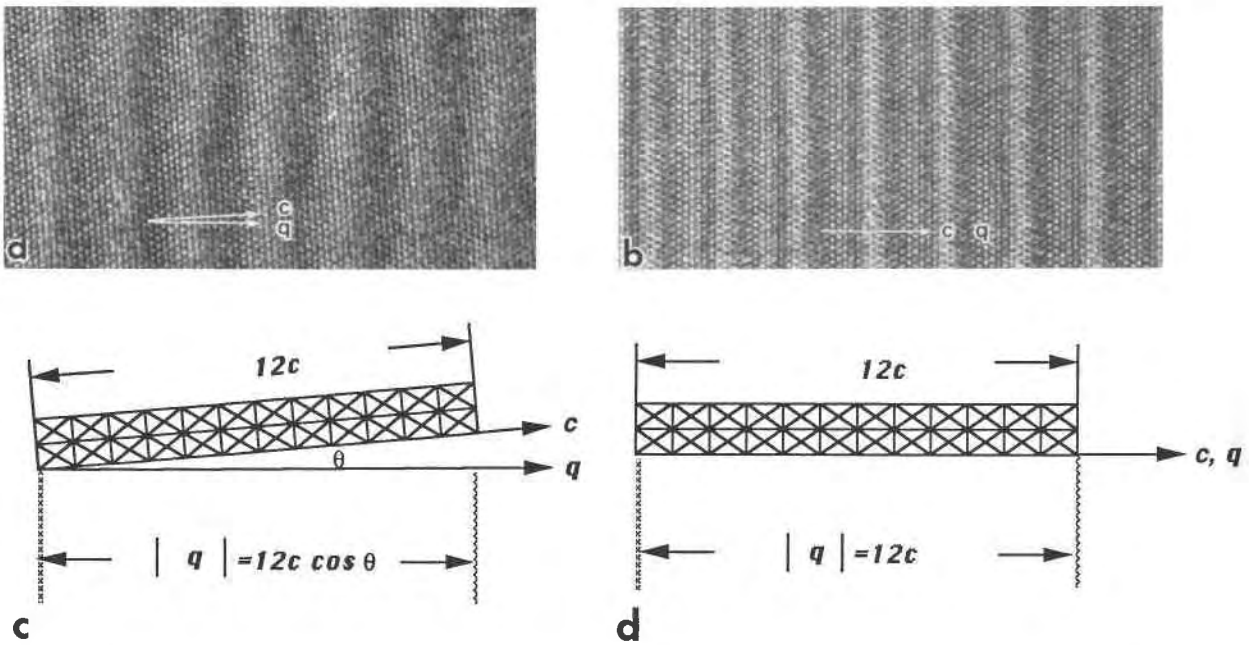

Fig. 5. Two [100] HRTEM images of the H sheets (**a**, **b**) and sketches (**c**, **d**) showing the crystal modulations. (**a**) Exterior and (**b**) close to the core of a cylindrical crystal. Sketches **c** and **d** correspond to images **a** and **b**, respectively. The θ represents the angle between **q** and the **c** axis of the H lattice. The wavelengths of the modulations are (**b**) longer where **q** is parallel to **c** than (**a**) where it is not.

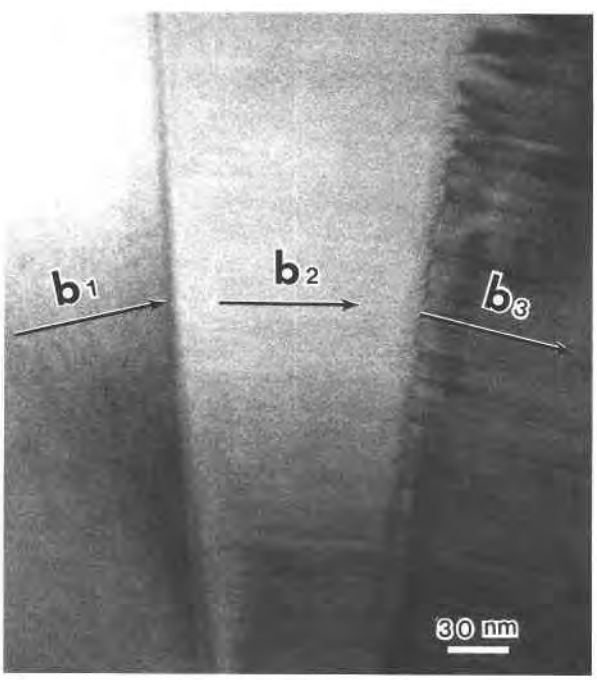

Fig. 6. A [001] TEM image of a region far from the core of the cylinder. Rather than being smoothly curved, the sheets are kinked. Regions b_1, b_2, and b_3 are domains having slightly different orientations.

T sheets, and so we were able to obtain separated [100] SAED patterns and HRTEM images for the two types of sheets. The direction of the modulation vector, **q**, that the two sheets have in common is determined by the relative orientations of the sheets. The vector **q** is consistent with a vector extending from the 002 reflection from the H sheets to 002 arising from the T sheets. Therefore this modulation can be used for determining the relative orientations and rotations of the sheets.

SAED and HRTEM studies show that the lattice parameters of the H and T sheets are constant across the width of a cylindrical crystal, although the relative rotations of the two sheets and thus the orientation of **q** change with radial position. The **b*** and **c*** axes in SAED patterns and the **b** and **c** axes in HRTEM images of the H and T sheets are closer in direction to each other at the interiors than at the exteriors of the cylinders (Figs. 3, 4). The vector **q** also shifts progressively toward **c** of both of the sheets near the cylinder cores, so that the **c*** axes of the H and T sheets and **q** are roughly parallel near the cylinder cores (Figs. 3c, 3f for reciprocal space and Figs. 4c, 4f for real space). The curvature of the cylindrite layers and the angular relation between the two types of sheets are directly correlated.

The vector **q** changes in both magnitude and direction with radial position. The modulation wavelengths near the cylinder cores are longer than those near the outsides of the crystals (Fig. 5). The H and T sheets retain the

proportion $13c_t/12c_h$ in the **c** direction. Where **q** is parallel to the **c** axes of the H and T sheets, the wavelength of the modulation is $12c_h$ and $13c_t$. Where the angle between **q** and the **c** axis of the H lattice is θ, or the angle between **q** and the **c** axis of the T lattice is ξ, the wavelength of the modulation is $|\mathbf{q}| = 12c_h\cos\theta = 13c_t\cos\xi$.

In some incommensurate modulated structures (e.g., γ-Na_2CO_3; van Aalst et al., 1976), the orientations of the satellite peaks change relative to the major substructure reflections when the crystal is heated. The effect is similar to the swing in **q** that can be observed in Figure 3. In order to determine whether the changes in cylindrite occur as a function of temperature, the crystals were heated in the electron microscope. The sample decomposed when heated to ~550 °C (1 °C/min), but **q** and the relation between the H and T sheets remained constant up to the decomposition temperature. Therefore, we conclude that the changes shown in Figures 3 and 4 are not a temperature effect.

The smooth curvatures of the H and T sheets are interrupted near both the exteriors and cores of the cylinders. Where the radius is large, the sheets form flat segments (Fig. 6), similar to the structures of Povlen-type chrysotile (Middleton and Whittaker, 1976) and the phases shown by Barbier et al. (1985). Smoothly curved sheets also do not form where the radius of curvature is very small, although the limiting radial value is uncertain. Figure 7, for example, shows that the smooth arcs of the layers disappear where the radius of curvature is less than ~16 nm (bottom part of the figure).

Conclusions

The basic structures of the two types of constituent sheets of cylindrite remain constant, independent of their radial positions in the crystal. However, their changing interrelationships with radial position give rise to both the incommensurate modulations and the unusual morphology of cylindrite. These relationships change with the radial position of the sheets within the crystal, i.e., with the amount of curvature of the sheets. Thus, the rotations of the sheets relative to one another increase from core to periphery of the cylindrical crystals, as does the deviation of **q**, the modulation vector, from **c** in the respective sheets.

Sheet curvatures are smooth except at maximum and minimum radial values, although the limiting radii seem to vary among different crystals, perhaps in response to compositional differences. For minimal curvature (maximum radius), the crystals develop planar segments, whereas for maximum curvature, near the crystal cores, the sheets develop somewhat contorted shapes that may also display kinking. The wavelengths of the modulations in our sample decrease from core to periphery of the crystal. There are clearly a variety of related chemical and structural features that combine to cause formation of the unusual cylindrical shape.

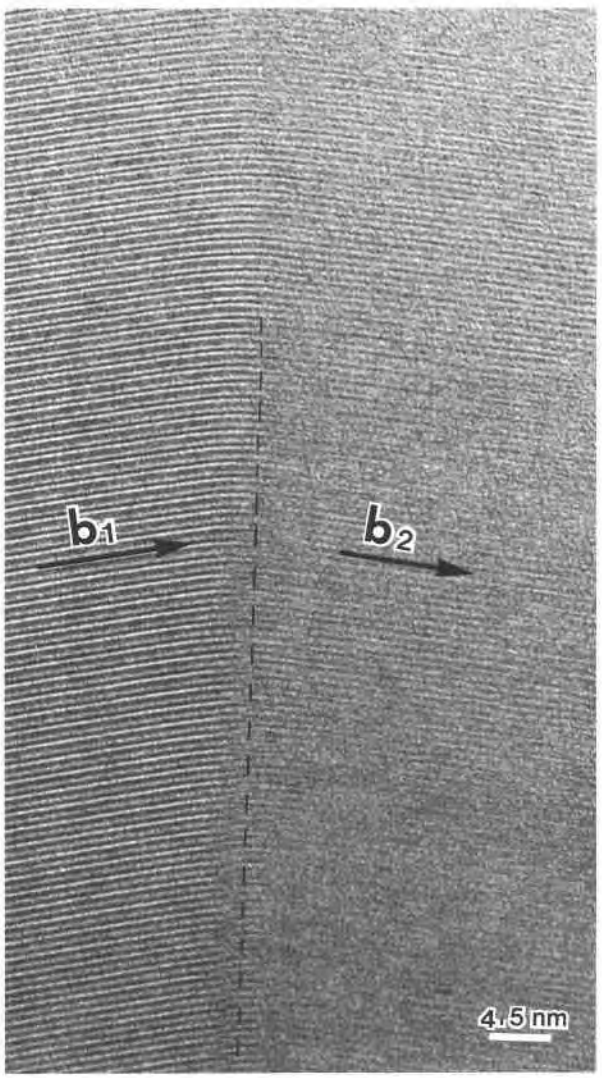

Fig. 7. A [001] HRTEM image showing the transition from a smooth (top) to kinked arc (bottom) near the cylinder core.

Acknowledgments

We thank J.C. Clark for help with electron microprobe analysis and K. Tomeoka, S.A. Kissin, and T. McCormick for helpful reviews. Electron microscopy was performed at the Facility for High Resolution Electron Microscopy at Arizona State University. The ASU HREM facility is supported by NSF and ASU, and this study was supported by NSF grant EAR-8708529. The electron microprobe was obtained through NSF grant EAR-8408168.

References cited

Barbier, J., Hiraga, K., Otero-Diaz, L.C., White, T.J., Williams, T.B., and Hyde, B.G. (1985) Electron microscope studies of some inorganic and mineral oxide and sulphide systems. Ultramicroscopy, 18, 211–234.

Belkin, H.E., and Libelo, E.L. (1987) Fibers and cylinders of cryptomelane-hollandite in Permian bedded salt, Palo Duro Basin, Texas. American Mineralogist, 72, 1211–1224.

Buseck, P.R., and Cowley, J.M. (1983) Modulated and intergrowth structures in minerals and electron microscope methods for their study. American Mineralogist, 68, 18–40.

Buseck, P.R., and Veblen, D.V. (1988) Mineralogy. In P.R. Buseck, J.M. Cowley, and L. Eyring, Eds., High-resolution transmission electron microscopy and associated techniques, p. 308–377. Oxford, New York.

Coppens, P., Maly, K., and Petricek, V. (1990) Composite crystals: What are they and why are they so common in the organic solid state? Molecular Crystals and Liquid Crystals, 181, 81–90.

Cowley, J.M. (1979) Retrospective introduction: What are modulated structures? In J.M. Cowley, J.B. Cohen, M.B. Salamon, and B.J. Wuensch, Eds., Modulated structures—1979, p. 3–9. American Institute of Physics, New York.

de Wolff, P.M., Janssen, T., and Janner, A. (1981) The superspace group for incommensurate crystal structures with a one-dimensional modulation. Acta Crystallographica, A37, 625–636.

Evans, H.T., Jr., and Allmann, R. (1968) The crystal structure and crystal chemistry of valleriite. Zeitschrift für Kristallographie, 127, 73–93.

Hirsch, P., Howie, A., Nicholson, R.B., Pashley, D.W., and Whelan, M.J. (1977) Electron microscopy of thin crystals, 563 p. Krieger, Melbourne, Florida.

Makovicky, E. (1971) Microstructure of cylindrite. Neues Jahrbuch für Mineralogie Monatshefte, 1971, 404–413.

——— (1974) Mineralogical data on cylindrite and incaite. Neues Jahrbuch für Mineralogie Monatshefte, 1974, 235–256.

Middleton, A.P., and Whittaker, E.J.W. (1976) The structure of Povlen-type chrysotile. Canadian Mineralogist, 14, 301–306.

Petricek, V., Maly, K., Coppens, P., Bu, X., Cisarova, I., and Frost-Jensen, A. (1991) The description and analysis of composite crystals. Acta Crystallographica, A47, 210–216.

Tomeoka, K., and Buseck, P.R. (1983) A new layered mineral from the Mighei carbonaceous chondrite. Nature, 306, 354–356.

van Aalst, W., den Hollander, J., Peterse, W.J.A.M., and de Wolff, P.M. (1976) The modulated structure of γ-Na_2CO_3 in a harmonic approximation. Acta Crystallographica, B32, 47–58.

Veblen, D.R., and Buseck, P.R. (1979) Serpentine minerals: Intergrowths and new combination structures. Science, 206, 1398–1399.

Wang, S. (1988) TEM study of frankeite and cylindrite. In H.G. Dickinson and P.J. Goodhew, Eds., Proceedings of the Ninth European Congress on Electron Microscopy, p. 331–332. York, England.

Wang, S., and Kuo, K.H. (1991) Crystal lattices and crystal chemistry of cylindrite group minerals. Acta Crystallographica, A4, 381–392.

Williams, T.B., and Hyde, B.G. (1988) Electron microscopy of cylindrite and franckeite. Physics and Chemistry of Minerals, 15, 521–544.

Yada, K. (1967) Study of chrysotile asbestos by a high resolution electron microscope. Acta Crystallographica, 23, 704–707.

——— (1971) Study of microstructure of chysotile asbestos by high resolution electron microscopy. Acta Crystallographica, A27, 659–664.

Zolensky, M.E., and Mackinnon, I.D.R. (1986) Microstructures of cylindrical tochilinites. American Mineralogist, 71, 1201–1209.

Manuscript received May 28, 1991
Manuscript accepted March 3, 1992